Title

Is spectral reflectance of the face a reliable biometric?

Journal

Optics Express, 23(12)

ISSN

1094-4087

Authors

Uzair, Muhammad

Mahmood, Arif

Shafait, Faisal

et al.

Publication Date

2015-06-15

DOI

10.1364/oe.23.015160

Peer reviewed

Is spectral reflectance of the face a reliable biometric?

Muhammad Uzair,[1,*] Arif Mahmood,[1] Faisal Shafait,[1] Christian Nansen[2] and Ajmal Mian[1]

[1]*Computer Science & Software Engineering, The University of Western Australia 35 Stirling Highway, Crawley, 6009 WA, Australia*
[2]*Department of Entomology and Nematology, University of California 95616 Davis, CA, USA*
[*]*muhammad.uzair@research.uwa.edu.au*

Abstract: Over a decade ago, Pan et al. [IEEE TPAMI 25, 1552 (2003)] performed face recognition using only the spectral reflectance of the face at six points and reported around 95% recognition rate. Since their database is private, no one has been able to replicate these results. Moreover, due to the unavailability of public datasets, there has been no detailed study in the literature on the viability of facial spectral reflectance for person identification. In this study, we introduce a new public database of facial spectral reflectance profiles measured with a high precision spectrometer. For each of the 40 subjects, spectral reflectance was measured at the same six points as Pan et al. [IEEE TPAMI 25, 1552 (2003)] in multiple sessions and with time lapse. Furthermore, we sample the facial spectral reflectance from two public hyperspectral face image datasets and analyzed the data using state of the art face classification techniques. The best performing classifier achieved the maximum rank-1 identification rate of 53.8%. We conclude that facial spectral reflectance alone is not a reliable biometric for unconstrained face recognition.

OCIS codes: (300.0300) Spectroscopy; (070.5010) Pattern recognition.

References and links

1. A. Jain, A. Ross, and S. Prabhakar, "An introduction to biometric recognition," IEEE Trans. on Circuits and Systems for Video Technology **14**, 4–20 (2004).
2. J. Pato and L. Millett, *Biometric Recognition: Challenges and Opportunities* (The National Academies, 2010).
3. J.-S. Fang, Q. Hao, D. Brady, B. Guenther, and K. Hsu, "A pyroelectric infrared biometric system for real-time walker recognition by use of a maximum likelihood principal components estimation (mlpce) method," Opt. Express **15**, 3271–3284 (2007).
4. A. Jain, P. Flynn, and A. Ross, *Handbook of Biometrics* (Springer-Verlag, 2007).
5. A. Mian, "Illumination invariant recognition and 3d reconstruction of faces using desktop optics," Opt. Express **19**, 7491–7506 (2011).
6. J. Hollas, *Modern Spectroscopy* (Wiley, 2004).
7. B. Stuart, *Infrared Spectroscopy: Fundamentals and Applications* (Wiley, 2004).
8. A. Thody, E. Higgins, K. Wakamatsu, S. Ito, S. Burchill, and J. Marks, "Phaeomelanin as well as eumelanin are present in human epidermis," J. Invest. Dermatol. **97**, 340–344 (1991).
9. A. Thody, E. Higgins, K. Wakamatsu, S. Ito, S. Burchill, and J. Marks, "Skin melanin, hemoglobin, and light scattering properties can be quantitatively assessed in vivo using diffuse reflectance spectroscopy," J. Invest. Dermatol. **117**, 1452–1457 (2001).
10. K. Nielsen, L. Zhao, J. Stamnes, K. Stamnes, and J. Moan, "The importance of the depth distribution of melanin in skin for DNA protection and other photobiological processes," J. Photoch. Photobio. B. **82**, 194–198 (2006).
11. A. Basiri, M. Nabili, S. Mathews, A. Libin, S. Groah, H. J. Noordmans, and J. C. Ramella-Roman, "Use of a multi-spectral camera in the characterization of skin wounds," Opt. Express **18**, 3244–3257 (2010).

#237187 - $15.00 USD Received 31 Mar 2015; revised 8 May 2015; accepted 15 May 2015; published 1 Jun 2015

12. D. Kapsokalyvas, N. Bruscino, D. Alfieri, V. de Giorgi, G. Cannarozzo, R. Cicchi, D. Massi, N. Pimpinelli, and F. S. Pavone, "Spectral morphological analysis of skin lesions with a polarization multispectral dermoscope," Opt. Express **21**, 4826–4840 (2013).
13. R. Anderson and J. Parrish, "The optics of human skin," J. Invest. Dermatol. **77**, 13–19 (1981).
14. M. Van Gemert, S. Jacques, H. Sterenborg, and W. Star, "Skin optics," IEEE Transactions on Biomedical Engineering **36**, 1146–1154 (1989).
15. D. Yudovsky and L. Pilon, "Retrieving skin properties from in vivo spectral reflectance measurements," J. Biophoton. **4**, 305–314 (2011).
16. R. Anderson and J. Parrish, "Optical properties of human skin," in *The Science of Photomedicine*, J. Regan and J. Parrish, eds. (Plenun, 1982), pp. 147–194.
17. Z. Pan, G. Healey, M. Prasad, and B. J. Tromberg, "Face recognition in hyperspectral images," IEEE Transactions on Pattern Analysis and Machine Intelligence **25**, 1552–1560 (2003).
18. D. Ryer, "Quest hierarchy for hyperspectral face recognition," Ph.D. thesis, Air Force Institute of Tech. (2012).
19. S. Robila, "Toward hyperspectral face recognition," SPIE, Image Proc: Algorithms and Sys. VI **6812**, 1–9 (2008).
20. Z. Pan, G. Healey, and B. J. Tromberg, "Comparison of spectral-only and spectral/spatial face recognition for personal identity verification," EURASIP Journal on Advances in Signal Processing **2009**, 943602 (2009).
21. W. Di, L. Zhang, D. Zhang, and Q. Pan, "Studies on hyperspectral face recognition in visible spectrumwith feature band selection," IEEE Transactions on Systems, Man, and Cybernetics, Part A **40**, 1354–1361 (2010).
22. L. Shen and S. Zheng, "Hyperspectral face recognition using 3d gabor wavelets," in "Int. Conference on Pattern Recognition," (2012), pp. 1574–1577.
23. M. Uzair, A. Mahmood, and A. Mian, "Hyperspectral face recognition using 3d-dct and partial least squares," in "Proceedings of British Machine Vision Conference," (2013), pp. 1–9.
24. CIE-CMFs, "http://cvrl.ioo.ucl.ac.ukcmfs.htm," .
25. L. Denes, P. Metes, and Y. Liu, "Hyperspectral face database," Tech. Rep. CMU-RI-TR-02-25, Robotics Institute, Pittsburgh, PA (2002).
26. Z. Khan, "Hyperspectral imaging and analysis for sparse reconstruction and recognition," Ph.D. thesis, Computer Science and Software Engineering, The University of Western Australia (2014).
27. S. Theodoridis and K. Koutroumbas, *Pattern Recognition* (Academic, 2010).
28. N. Cristianini and J. Shawe-Taylor, *An Introduction to Support Vector Machines and Other Kernel-Based Learning Methods* (Cambridge University, 2000).
29. B. Scholkopf and A. J. Smola, *Learning with Kernels: Support Vector Machines, Regularization, Optimization, and Beyond* (MIT, 2001).
30. C. Chang and J. Lin, "Libsvm: A library for support vector machines," ACM Trans. Intell. Syst. Tech. **2** (2011).
31. G. Baudat and F. Anouar, "Generalized discriminant analysis using a kernel approach," Neural Computation **12**, 2385–2404 (2000).
32. L. Clemmensen, T. Hastie, D. Witten, and B. Ersb∅ll, "Sparse discriminant analysis," Technometrics **53**, 406–413 (2011).
33. J. Kittler, M. Hatef, R. P. W. Duin, and J. Matas, "On combining classifiers," IEEE Transactions on Pattern Analysis and Machine Intelligence **20**, 226–239 (1998).
34. P. Phillips, H. Moon, S. Rizvi, and P. Rauss, "The feret evaluation methodology for face-recognition algorithms," IEEE Transactions on Pattern Analysis and Machine Intelligence **22**, 1090–1104 (2000).
35. R. Ruiz-Maldonado and M. Orozco-Convarrubias, "Postinflammatory hypopigmentation and hyperpigmentation," Seminars in Cutaneous Medicine and Surgery **16**, 36–43 (1997).
36. G. Zonios and A. Dimou, "Melanin optical properties provide evidence for chemical and structural disorder in vivo," Opt. Express **16**, 8263–8268 (2008).
37. K. Zuzak, M. Schaeberle, E. N. Lewis, and I. Levin, "Visible reflectance hyperspectral imaging: Characterization of a noninvasive, in vivo system for determining tissue perfusion," Analytical Chemistry **74**, 2021–2028 (2002).
38. Y. Yuan and P. Relue, "Enzymatic degradation of human skin dermis revealed by fluorescence and reflectance spectroscopy," Opt. Express **16**, 9857–9868 (2008).
39. K. Nielsen, L. Zhao, J. Stamnes, K. Stamnes, and J. Moan, "Reflectance spectra of pigmented and nonpigmented skin in the UV spectral region," Photochemistry and Photobiology **80**, 450–455 (2004).
40. T. Gambichler, J. Huyn, N. Tomi, G. Moussa, C. Moll, A. Sommer, P. Altmeyer, and K. Hoffmann, "A comparative pilot study on ultraviolet-induced skin changes assessed by noninvasive imaging techniques in vivo," Photochemistry and Photobiology **82**, 1103–1107 (2006).
41. J. M∅ller, T. Poulsen, and H. Wulf, "Epidermal thickness at different body sites: Relationship to age, gender, pigmentation, blood content, skin type and smoking habits," Acta Dermato Venereologica **83**, 410–413 (2003).

1. Introduction

Biometric identification refers to the recognition of target objects by analysing and quantifying their physiological, chemical or behavioral characteristics [1]. Biometric identification has a

#237187 - $15.00 USD Received 31 Mar 2015; revised 8 May 2015; accepted 15 May 2015; published 1 Jun 2015

wide range of applications in surveillance, security, border control, access control and law enforcement [2]. Any human physiological and/or behavioral characteristic that has the properties of universality, distinctiveness, permanence and quantitative measurability can be used as a biometric [3]. A practical biometric identification system should be accurate, non-invasive, socially acceptable, cost-effective and robust to spoofing attacks [1]. Common biometric modalities for human identification include face images, iris/retinal scans, finger/palm prints, hand geometry and speech signals [4, 5].

Spectroscopy is the study of absorption, reflection, or scattering of the electromagnetic energy by a material in order to qualitatively or quantitatively characterize its composition and identity [6]. In spectroscopy, usually the transmitted or reflected electromagnetic energy is measured by a spectroscopic device and is then represented by a spectrum as a function of wavelength versus intensity, distance and projection angle of the electromagnetic energy [7]. This spectrum is also called the spectral response of the material and provides hints about the chemical composition or physical behaviour of the material.

The epidermal and dermal layers of human skin constitute a scattering medium and contain tissue chromophores such as melanin and oxygenated or deoxygenated hemoglobin and other chemicals such as β-carotene [8–10]. Reflectance spectroscopy involves the measurement and study of the reflected electromagnetic energy from a material. Reflectance spectroscopy of the skin surface can be performed non-invasively to sense the subsurface skin chemical distributions [9] and has been used by various researchers [11–16] for skin characterization.

Assuming that the spectral reflectance features of human skin are somewhat unique among all humans and also consistent over time, then it may be possible to deploy reflectance spectroscopy for human identification. Pan et al. [17] acquired reflectance data from 200 human subjects and were able to identify individuals with about 95% accuracy. The experimental setup consisted of human faces being imaged in a single session (no time lapse), and spectral reflectance features were acquired in 33 spectral bands (10 nm band width). A session means a single sitting in which the spectral reflectance profiles of a subject are measured. However, the dataset is not publicly available; therefore, it has not been possible to validate their research results. In fact, other researchers have been unable to replicate these results on their own databases [18]. Therefore, the question whether spectral reflectance of the human face is a viable biometric is still and open question.

In this paper, we perform reflectance spectroscopy to investigate practical significance of human facial spectral reflectance for person identification. We present a database of high resolution facial spectral reflectance features of 40 human subjects. Each spectral reflectance profile has 1761 bands with 0.5nm bandwidth in wavelength range of 220-1100nm. The spectral reflectance of each subject is measured in multiple sessions and multiple times in each session. The time lapse between each session varies from one day to nine months. For data collection, a high resolution, high accuracy spectrometer under precisely calibrated lighting conditions is used. The performance of the facial spectral response for person identification is evaluated using state-of-the-art classification algorithms. In our experiments, the best performing classifier achieved the maximum rank-1 identification rate of 53.8%. This suggests that the facial spectral reflectance alone does not provide good unconstrained human identification accuracy. We believe that our new database and results are very important in order to advance the research in the area of spectral reflectance based face recognition in particular and spectral biometrics in general.

2. Related work

There are only two previous studies on the use of spectral reflectance for biometric recognition. Both studies use hyperspectral cameras for reflectance spectroscopy. The first study on spectral reflectance based face recognition was conducted by Pan et al. [17] using 2D hyperspectral

#237187 - $15.00 USD Received 31 Mar 2015; revised 8 May 2015; accepted 15 May 2015; published 1 Jun 2015

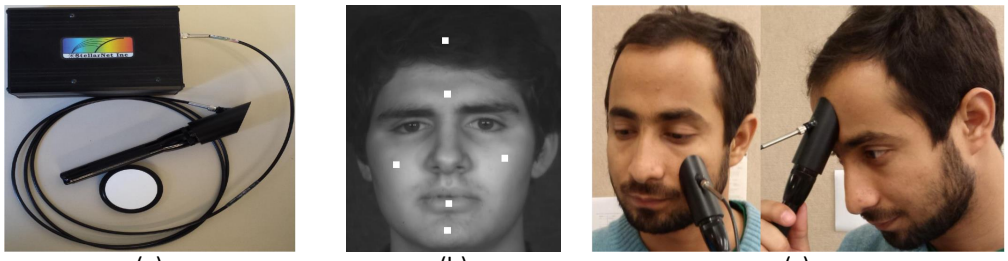

(a) (b) (c)

Fig. 1. (a) StellarNet CXR-SR-50 spectrometer and armoured reflectance fiber with 600μm diameter. Apogee AS-003 reflectance probe with built-in light source. (b) Six facial points from where the spectral reflectance profiles are sampled. (c) The measurement procedure.

images in the near-infrared range (700-1000nm). They manually sampled the 31 dimensional (31 band) spectral reflectances from hand picked locations on the hair, forehead, cheeks, lips and chin of each subject (Fig. 1(b)). The spectral reflectance profiles were classified using the Mahalanobis distance based classifier to perform face recognition. Robila [19] extended the previous study by expanding the wavelength range and using hyperspectral images of 120 bands (400nm-900nm). He also used spectral reflectance profiles of different face regions but compared them using the spectral angle based distance. However, his experiments involved a small proprietary database of only eight subjects.

Some researchers used both spatial and spectral features of hyperspectral images for face recognition. Pan et al. [20] extracted spatio-spectral features, called the 2D spectral-face, by recursively sampling each subsequent pixel from the next band. Di et al. [21] used 2D PCA to extract low dimensional features from hyperspectral cubes. The 2D PCA based features were then classified for face recognition. They also introduced a public hyperspectral face database PolyU-HSFD [21] in the visible range (400-720nm) containing 25 subjects. However, the signal to noise ratio in individual bands of this database is very low making the spectral response unreliable. Shen and Zheng [22] extracted spatiospectral features from each hyperspectral cube using 3D-Gabor wavelets. Uzair et al. [23] extracted spatiospectral features using the classical 3D-DCT transform and classified them using Partial Least Squares. They also introduced a public hyperspectral face database UWA-HSFD [23] containing 70 subjects captured in the visible range (400-720nm). The UWA-HSFD database is less noisy compared to the PolyU-HSFD, however, the spectral resolution is low consisting of only 33 bands covering only the visible range (400-720nm). All these studies utilize both the spatial and the spectral features. Therefore, the role of spectral features alone for face recognition is not clear.

The databases used in previous studies are noisy [21], captured in a constrained setup, have low spectral resolution and are not publicly available [17]. Therefore, the results from these databases are limited and it is inconclusive as to whether the facial spectral reflectance alone can be used as a unique person identifier. Moreover, these datasets do not encourage further studies or comparisons on spectral reflectance based face recognition. In contrast, we introduce the first ever public database of high resolution calibrated facial spectral reflectances that are measured by a high precision spectrometer in an unconstrained manner. Our experimental results also provide insight into the role of spectral reflectance for biometric recognition.

3. Database collection

We used the StellearNet CXR-SR-50 spectrometer for our database collection (Fig. 1(a)) which can measure the spectral response of a material in the wavelength range of 220nm to 1100nm with a step size of 0.5nm. The spectral response is recorded by connecting the spectrometer to a personal computer via USB port using a fiber optic cable attached to the standard SMA905

#237187 - $15.00 USD Received 31 Mar 2015; revised 8 May 2015; accepted 15 May 2015; published 1 Jun 2015

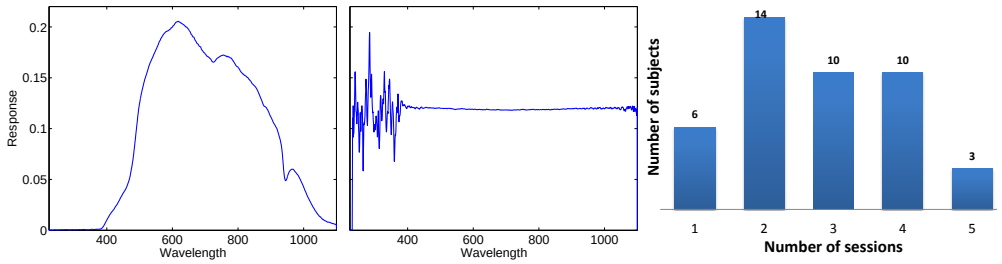

Fig. 2. (Left to right) Spectral power distribution of the illumination. Normalized spectral reflectance of the standard white that we use for calibration. The number participants in different sessions of the UWA Facial Spectral Reflectance Database (UWA-FSRD).

connector. We use an armoured, single strand, multimode, 2 meters fiber optic cable supplied with the spectrometer by StellarNet. The detection fiber has a diameter of 600μm and an operating range of 190-2200nm. We used the Apogee Instruments AS-003 reflectance probe with built-in illumination which is designed specially for accurate spectroscopy. The main advantage of choosing the reflectance probe is that it blocks the ambient illumination and ensures that a constant distance and angle is maintained with the sample. The probe holder maintains a constant distance of 20mm between the sample and the detection fibre. At this distance, the fiber detection area is 51.0mm^2. Figure 2(a) shows the Spectral Power Distribution (SPD) of the illumination provided with the reflectance probe. We calibrate the spectrometer in the beginning of each session with standard white and standard black materials. For calibration, the standard white provided by the StellarNet is used. This standard white reflects over 99% of the incident light (Fig. 2(a)). We use the SpectraWiz software for calibration and reflectance measurement and keep the same calibration settings in our entire experiment. We set the detector integration time to 170ms and store the average of 5 scans.

With the calibrated spectrometer, we measure the spectral reflectance from the same six skin regions those selected by Pan et al. [17]. The regions include forehead, right cheek, left cheek, lips, chin and hair (Fig. 1(b)). To measure the spectral reflectance, we place the probe softly (without pressing) (Fig. 1(c)) on the skin region to be measured and capture the spectral reflectance through the SpectraWiz software.

3.1. Database details

We have collected a database of 325 spectral reflectance profiles of six facial regions from 40 subjects (5 females, 35 males). We call our database the UWA Facial Spectral Reflectance Database (UWA-FSRD) (publicly available at: `http://www.csse.uwa.edu.au/~ajmal/databases.html`). Our database contains subjects from six different ethnicities including African (2), Caucasian (12), Chinese (5), Indian (17), Middle Eastern and South American (1). The ages of the subjects fall in the range 20-45 years. The spectral reflectances of each subject are measured in multiple sessions. Figure 2(b) summarizes the number of subjects present in different sessions. Specifically, a total of ten subjects are with four or more sessions, ten with three sessions, 14 with two sessions and the remaining six subjects are with one session. In each session we acquired 2-13 spectral reflectance profiles of each facial region within a close proximity.

The time lapse between two sessions for a subject varies between a minimum of one day and a maximum of more than nine months. This setting enables us to study the permanence of the spectral reflectance biometric over time. Note that our main focus is on biometric identification where constraints on the subjects physical conditions are not desirable. Therefore, we do not impose any constraints on the subjects such as cleaning the skin or shaving before data collection.

#237187 - $15.00 USD Received 31 Mar 2015; revised 8 May 2015; accepted 15 May 2015; published 1 Jun 2015

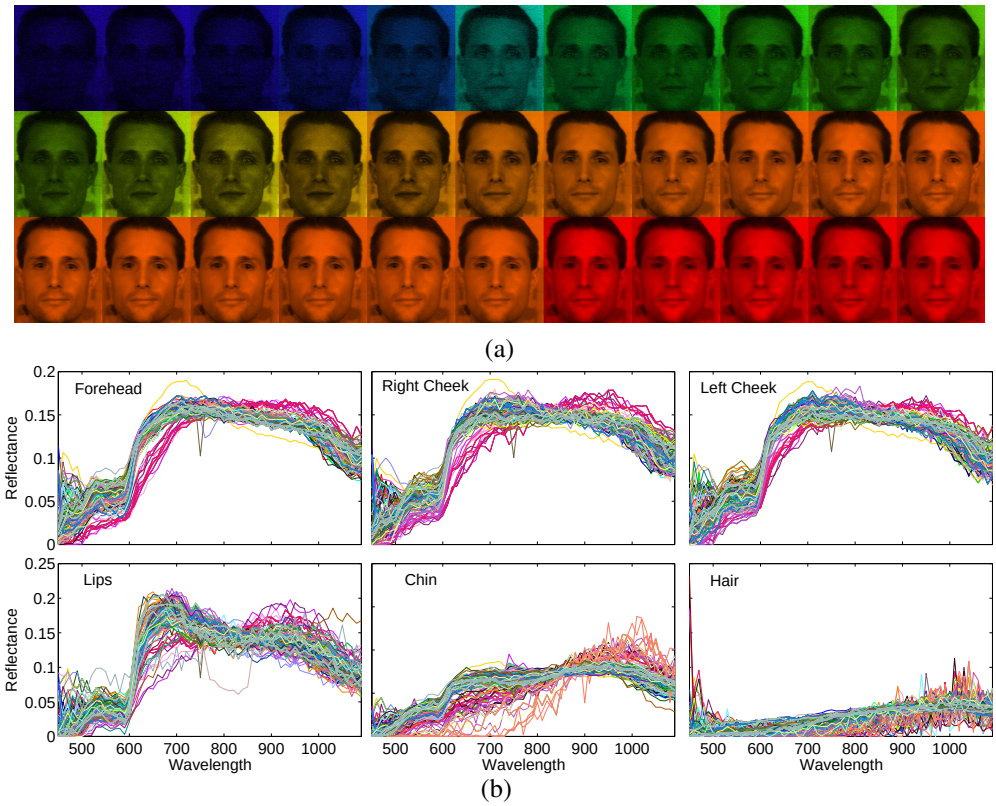

Fig. 3. (a) A hyperspectral face cube from the CMU-HSFD (bands from 450nm to 770nm). Each band is rendered as RGB using the standard CIE Color Matching Functions [24]. (b) Normalized spectral reflectance profiles of six facial regions of 48 subjects in the CMU-HSFD.

3.2. Facial spectral reflectance sampling from existing hyperspectral databases

In addition to our spectrometer based database, we also used two existing hyperspectral face image databases in our experiments (Table 1). These databases were captured with hyperspectral cameras and contain two dimensional (2D) images of the face at multiple wavelengths. Therefore, both the spatial and spectral information of the face are available. However, we only sample the spectral information of six facial points for our experiments.

CMU-HSFD: The first database is the CMU Hyperspectral Face Database (CMU-HSFD) [25] (Fig. 3(a)) acquired with a prototype spectro-polarimetric camera. Each hyperspectral image cube contains 65 bands covering the spectral range of 450-1090nm range with a step size of 10nm. For illumination, three identical lamps with 600W halogen bulbs were used. The database contains 48 subjects; each subject has 4 to 20 cubes acquired at different sessions and different lighting combinations. We used only the images acquired with all lights turned on. In order to sample the calibrated spectral reflectance, we normalized the hyperspectral images

Table 1. Details of the databases used in our study.

Database	Type	Size	Subjects	Spectra	Spectral range	Step size
CMU-HSFD [25]	Images	640×80×65	48	882	450-1090nm	10nm
UWA-HSFD [23]	Images	1024×1024×33	70	720	400-720nm	10nm
UWA-FSRD	Spectra	6×1761	40	325	220-1100nm	0.5nm

#237187 - $15.00 USD Received 31 Mar 2015; revised 8 May 2015; accepted 15 May 2015; published 1 Jun 2015

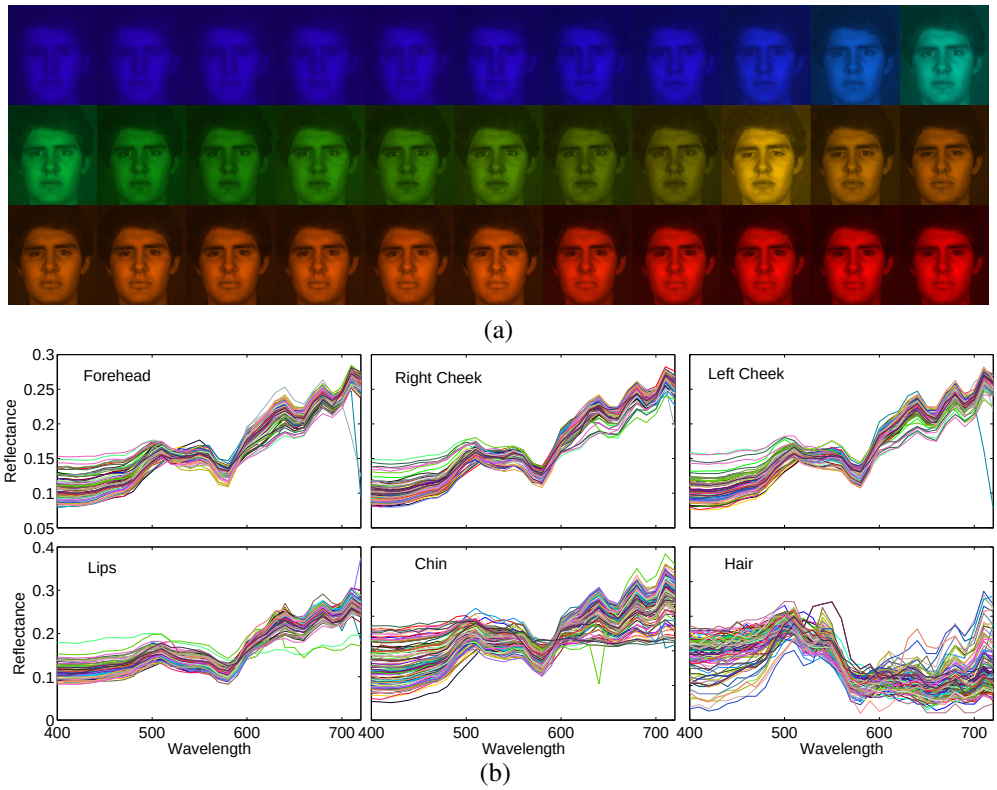

Fig. 4. (a) A hyperspectral face cube from the UWA-HSFD. Each band is rendered as RGB using the standard CIE Color Matching Functions [24]. (b) Normalized spectral reflectance profiles of six facial regions of 70 subjects in the UWA-HSFD.

using the provided calibration patch in the images. Our experimental data consists of 147 hyperspectral images of 48 subjects where each subject has 1 to 5 images (Table 1). Figure 3(b) shows the normalized reflectance profiles of six facial regions of the 48 subjects in CMU-HSFD.

UWA-HSFD: The second database is our local UWA-Hyperspectral Face Database (UWA-HSFD) (Fig. 4(a)) acquired with the CRI's VariSpec LCTF integrated with a photon focus camera. Each hyperspectral image cube contains 33 bands covering the spectral range of 400-720nm with a 10nm step. The noise level in this database is relatively lower because an improved calibration algorithm [26] is used that automatically adapts the camera exposure time to the transmittance of the filter, illumination intensity and CCD sensitivity in each band. In order to sample the exact spectral reflectance, the camera is calibrated with standard white in the beginning of each imaging season. The UWA-HSFD consists of 120 hyperspectral images of 70 subjects.(Table 1). The time lapse between imaging sessions for a subject in the UWA-HSFD varies from one week to 12 months. Figure 4(b) shows the normalized reflectance profiles of six facial regions of the 70 subjects in UWA-HSFD.

From each subject in the UWA-HSFD and CMU-HSFD, we manually sample the spectral reflectances of six facial points including forehead, left cheek, right cheek, lips, chin and hair. We use the average spectral reflectance of 5 adjacent square regions of size 17×17 pixels arranged in a cross pattern to represent hair, forehead and cheeks. For lips we use square regions of size $9\times$ 9 pixels. Based on the relationship between the average physical distance and the average number of pixels between the eye centers, a pixel in the UWA-HSFD and CMU-HSFD roughly corresponds to 0.18mm^2 and 0.32mm^2 respectively. Therefore, the physical area cov-

#237187 - $15.00 USD Received 31 Mar 2015; revised 8 May 2015; accepted 15 May 2015; published 1 Jun 2015

ered by 17x17 pixels roughly equals to 52.02mm^2 for UWA-HSFD and 92.48mm^2 for CMU-HSFD. Recall that the fiber detection area in UWA-FSRD is 51.0mm^2 (see Section 3). In the case of UWA-HSFD each spectral reflectance vector is 33-dimensional, while for CMU-HSFD database the spectral reflectance vector is 65-dimensional. Theses spectral reflectances are ℓ_2 normalized and subsequently used for classification. The normalization reduces scaling effects in the spectral responses due to the sensor noise.

4. Recognition based on the facial spectral reflectance

In this section, we explain the machine learning algorithms we used for performing recognition using the facial spectral responses. Let $\mathbf{s}_r = [s_r(\lambda_1), s_r(\lambda_2), ..., s_r(\lambda_p)] \in \mathbb{R}^p$ be the spectral response vector of the facial region r that samples the reflected energy from p wavelengths. Let $\mathbf{G}_r = \{\mathbf{s}_r^j\}_{j=1}^g \in \mathbb{R}^{p\times g}$ be the gallery containing g normalized spectral reflectances of facial region r. Let c be the number of subject classes such that $m_j \geq 1$ is the number of spectral responses for each class, $g = \sum_{j=1}^c m_j$ and $\mathbf{Y} = \{y^j\}_{j=1}^g$ be the class labels of the spectral responses in $\mathbf{G}_r$. Let $\mathbf{s}_r^t \in \mathbb{R}^p$ be the test spectral response. The problem of spectral reflectance based face recognition involves estimating the label y_r^t of $\mathbf{s}_r^t$ given the labelled gallery $\mathbf{G}_r$.

We choose a mix of simple and more sophisticated classification algorithms for recognition. The simple algorithms include Nearest Neighbor (NN) and Support Vector Machines (SVM) which perform classification on the original spectral reflectance vectors. The sophisticated ones include Kernel Linear Discriminant Analysis (KLDA) and Sparse Discriminant Analysis (SDA) that extract discriminant features from the reflectance profiles.

Mahalanobis distance based nearest neighbour classifier: The Mahalanobis distance d between two spectral response vectors $\mathbf{s}_r^i$ and $\mathbf{s}_r^j$ is defined as [27]

$$d = (\mathbf{s}_r^i - \mathbf{s}_r^j)^\top \mathbf{C}_r^{-1} (\mathbf{s}_r^i - \mathbf{s}_r^j) \tag{1}$$

where $\mathbf{C}_r$ is the $p \times p$ covariance matrix estimated from the training spectral responses of facial region r. Since the amount of training data is limited, we estimate $\mathbf{C}_r$ to be a diagonal matrix with elements that correspond to the variance of each wavelength in the spectra. To classify $\mathbf{s}_r^t$ we first calculate the distance (d) from $\mathbf{s}_r^t$ to each of the samples in $\mathbf{G}_r$ and obtain a score vector $\mathbf{e}_r \in \mathbb{R}^g$. Then, y_r^t is estimated as the label of the class for which the distance in $\mathbf{e}_r$ is minimum.

Support vector machines (SVM) Support Vector Machine is an efficient classification algorithm designed for binary classification problems where we assume that there are g training samples $\{\mathbf{s}_r^j\}_{j=1}^g$ with labels $y^j \in \{1, -1\}$. SVM finds a hyper-plane that separates the two classes with the largest margin by solving the following optimization problem:

$$\begin{aligned} &\min_{\mathbf{w},b,\xi} \left(\frac{1}{2}\mathbf{w}^\top \mathbf{w} + C\sum_j \xi^j \right) \\ &s.t.\ \ y^j(\mathbf{w}\mathbf{s}_r^j + b) \geq 1 - \xi^j, \xi^j \geq 0 \end{aligned} \tag{2}$$

Where C is the penalty parameter, $\mathbf{w}$ and b are the parameters of the hyperplane and ξ^j are auxiliary variables that allow to handle non-separable problems. For kernel SVM, the constraint can be replaced by $y^j(\mathbf{w}\phi(\mathbf{s}_r^j) + b) \geq 1 - \xi^j, \xi^j \geq 0$ to find the hyper-plane in a higher dimensional space. Once the parameters of the hyper-plane are obtained, the label y_r^t of the test spectral reflectance $\mathbf{s}_r^t$ is estimated using the sign of $\frac{\mathbf{w}\mathbf{s}_r^t + b}{\|\mathbf{w}\|}$. Since our experiments involve the classification of 40 subjects (classes), therefore; we extend the binary SVM to multi-class classification using a one-versus-all approach. For a detailed explanation of the SVM algorithm, we refer the reader to [28, 29]. We used the LibSVM [30] library to compute the parameters of the hyper-plane.

#237187 - $15.00 USD Received 31 Mar 2015; revised 8 May 2015; accepted 15 May 2015; published 1 Jun 2015

Kernel linear discriminant analysis (KLDA) extracts discriminative and low dimensional features from the data. KLDA is especially useful in increasing the between class discrimination when the classes are not linearly separable. It projects the p dimensional spectral response features in $\mathbf{G}_r$ to a $c-1$ dimensional subspace where classification is performed.

Let ϕ be a non-linear mapping function that maps the spectral reflectances $\mathbf{s}_r^i \in \mathbb{R}^p$ to a high dimensional feature space $\phi : \mathbb{R}^p \mapsto \mathscr{H}$. The features belonging to different classes are better discriminated in the high dimensional non-linear space $\mathscr{H}$. A kernel matrix $\mathbf{K}_r \in \mathbb{R}^{g\times g}$ can be computed by means of dot products in the high dimensional feature space. However, rather than explicitly mapping the data to $\mathscr{H}$ by implementing the non-linear mapping ϕ, the kernel matrix is often computed by choosing a valid kernel function: $\mathbf{K}_r(i,j) = k(\mathbf{s}_r^i, \mathbf{s}_r^j)$. We choose the polynomial kernel function $k(\mathbf{s}_r^i, \mathbf{s}_r^j) = (\mathbf{s}_r^i.\mathbf{s}_r^j)^\beta$, where $(\cdot)$ means dot product and β is the order of polynomial.

Once $\mathbf{K}_r$ is computed, KLDA seeks to solve the following optimization problem [31]

$$\alpha_{opt} = \arg\max \frac{\alpha^\top \mathbf{K}_r \mathbf{W} \mathbf{K}_r \alpha}{\alpha^\top \mathbf{K}_r \mathbf{K}_r \alpha}, \tag{3}$$

where $\alpha = [\alpha_1, ..., \alpha_g]^\top$. $\mathbf{W} \in \mathbb{R}^{g\times g}$ is a block diagonal matrix:$\mathbf{W} = diag\{\mathbf{W}_1, \mathbf{W}_2, ..., \mathbf{W}_c\}$, where $\mathbf{W}_j \in \mathbb{R}^{m_j \times m_j}$ is a matrix with all elements equal to $\frac{1}{m_j}$. The optimal α is given by the largest eigenvectors of $(\mathbf{K}_r\mathbf{K}_r + \varepsilon\mathbf{I})^{-1}(\mathbf{K}_r\mathbf{W}\mathbf{K}_r)\alpha = \lambda\alpha$. By selecting the $(c-1)$ dominant eigenvectors, we obtain a transformation matrix $\Lambda = [\alpha_1, ..., \alpha_{c-1}] \in \mathbb{R}^{p\times(c-1)}$. The gallery $\mathbf{G}_r$ is then projected on Λ to obtain a low dimensional representation $\widehat{\mathbf{G}}_r = \Lambda^\top \mathbf{G}_r$.

To predict the label of a test spectral reflectance $\mathbf{s}_r^t$, first the $c-1$ dimensional KLDA feature $\mathbf{z}_r^t$ is computed by $\mathbf{z}_r^t = \Lambda^\top \mathbf{K}_r^t$. Here $\mathbf{K}_r^t = [k(\mathbf{s}_r^t, \mathbf{s}_r^1), ..., k(\mathbf{s}_r^t, \mathbf{s}_r^g)] \in \mathbb{R}^{c-1}$. Then the Euclidean distance is computed from $\mathbf{z}_r^t$ to each of the low dimensional samples in $\widehat{\mathbf{G}}_r$ and a score vector $\mathbf{e}_r \in \mathbb{R}^g$ is obtained. Finally, y_r^t is estimated as the label of the class for which the distance in $\mathbf{e}_r$ is minimum.

Sparse discriminant analysis (SDA) extracts discriminative features as sparse combinations of the input data. In our case of reflectance spectra, SDA will use a sparse combination of the bands to extract features. Thus, SDA has an inbuilt feature/band selection step. SDA is particularly useful when the number of variables are greater than the number of samples in the training set. Let $\mathbf{Q} \in \mathbb{R}^{g\times c}$ denote a matrix of dummy variables for the c classes; Q_{ij} is an indicator variable for whether the i-th observation belongs to the j-th class. SDA is formulated by combining the optimal scoring criterion with the elastic net [32]

$$\begin{aligned} &\min_{\beta_i,\theta_i} \left(\|\mathbf{Q}\theta_i - \mathbf{G}_r^\top \beta_i\| + \lambda\|\beta_i\|_1 + \gamma\|\beta_i\|^2 \right) \\ &s.t.\ \ \frac{1}{g}\theta_i^\top \mathbf{Q}^\top \mathbf{Q}\theta_i = 1, \theta_i^\top \mathbf{Q}^\top \mathbf{Q}\theta_l = 0 \forall l < i \end{aligned} \tag{4}$$

where θ_i be the c-vector of scores for the c classes, and β_i is a p-vector representing variable coefficients for the p features. The problem is solved using the iterative algorithm presented in [32] to obtain $\mathbf{B} = [\beta_1, ..., \beta_{(c-1)}]$. The gallery $\mathbf{G}_r$ is then projected on $\mathbf{B}$ to obtain a low dimensional representation and discriminative features $\widehat{\mathbf{G}}_r = \mathbf{B}^\top \mathbf{G}_r$.

To predict the label of a test spectral reflectance $\mathbf{s}_r^t$, first the $c-1$ dimensional SDA features $\mathbf{z}_r^t$ are computed by $\mathbf{z}_r^t = \mathbf{B}^\top \mathbf{z}_r^t$. Then the Euclidean distance from $\mathbf{z}_r^t$ to each of the low dimensional samples in $\widehat{\mathbf{G}}_r$ is calculated and a score vector $\mathbf{e}_r \in \mathbb{R}^g$ is obtained. Finally, y_r^t is estimated as the label of the class for which the distance in $\mathbf{e}_r$ is minimum.

#237187 - $15.00 USD Received 31 Mar 2015; revised 8 May 2015; accepted 15 May 2015; published 1 Jun 2015

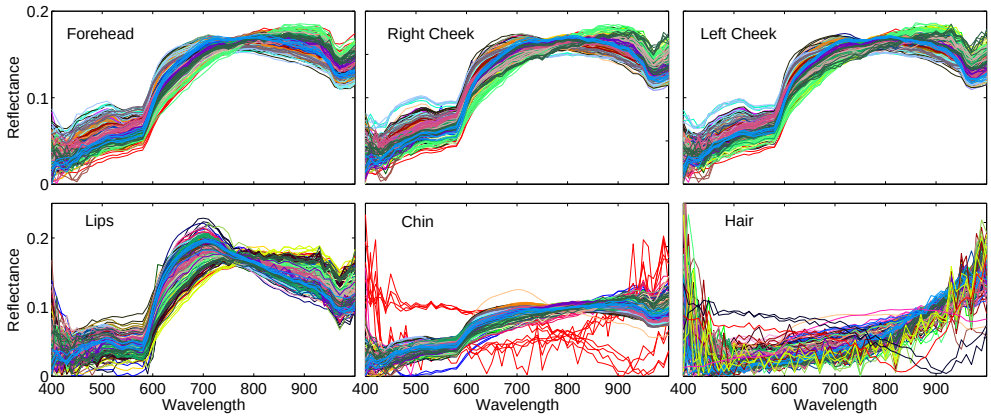

Fig. 5. Normalized spectral responses of six facial regions of 40 subjects in our UWA-FSRD. The very different spectral reflectance profiles of the chin are from individuals with facial hairs.

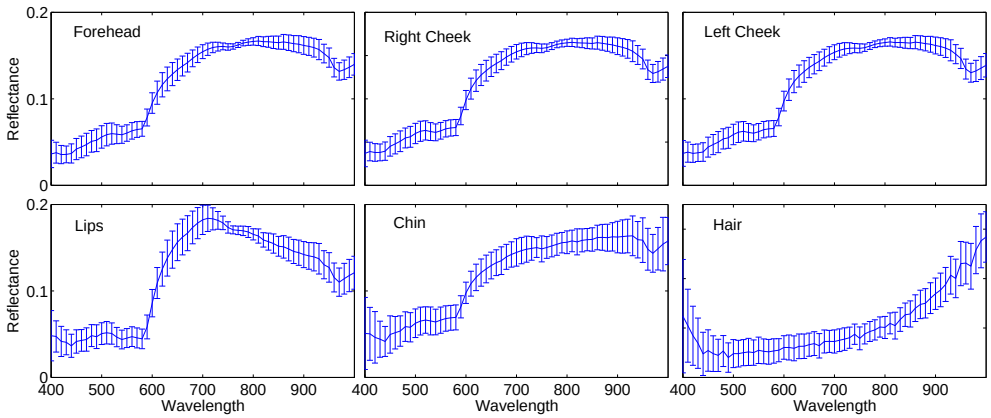

Fig. 6. Average and standard deviations of the spectral reflectances of the six facial regions of 40 subjects in our UWA-FSRD.

Score level fusion: Since we have $r = 6$ facial regions of each subject, we train a separate classifier for each region and combine their result at the score level. We use the sum rule of classifier fusion due to its excellent performance for combining classifiers [33]. The sum rule of classifier score fusion uses the simple sum operator to combine the output scores of multiple classifiers. For a test subject, the r test spectral reflectances $\{\mathbf{s}_k^t\}_{k=1}^r$ generate r score vectors $\{\mathbf{e}_r\}_{k=1}^r$. We first normalize each score vector $\mathbf{e}_r$ separately using min-max normalization. Next, we use the sum operator to compute the fused score vector i.e. $\mathbf{f} = \sum_{k=1}^r \mathbf{e}_r$. Finally, the test subject is assigned the label of the class for which the distance in $\mathbf{f}$ is minimum.

5. Experiments

We do not use ultraviolet illumination because skin spectroscopy in the ultraviolet spectrum is unsafe. Moreover, our probe light has very low power above 1000nm (Fig. 1) making measurements above this range noisy. Light sources and spectrometers that operate in a broader spectrum are expensive and are less likely to be used in a practical spectral reflectance based face recognition system. Therefore, in our experiments we only consider the reflectance profiles in the 400-1000nm range. The ℓ_2 normalized spectral reflectances of the right cheek, lips and hair of the 40 subjects in our database are shown in Fig. 5. Figure 6 shows the average spectral

#237187 - $15.00 USD Received 31 Mar 2015; revised 8 May 2015; accepted 15 May 2015; published 1 Jun 2015

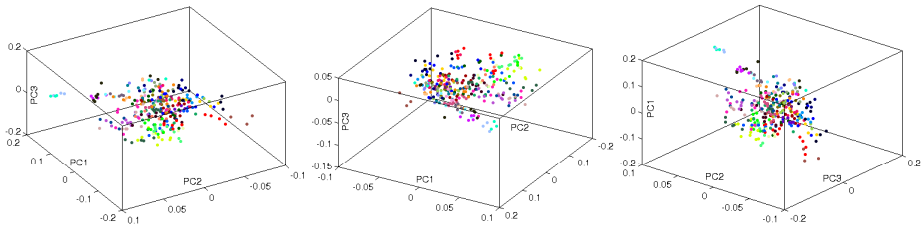

Fig. 7. Spectral reflectance features of the right cheek projected to a 3D PCA space. The dimensions represent the three dominant principal components (PCs) and each dot represents the reflectance profile of a subject. Each subject is represented by a different color. Notice the difficulty of separating different subjects.

reflectance profiles of the 40 subjects in our UWA-FSRD database. The standard deviations along the profile curves are also shows using error bars. It can be observed that the spectral reflectance curves of all subjects follow a similar pattern. To visualize the manifold structure of spectral reflectance features, we performed Principal Component Analysis (PCA) on our entire database. Figure 7 shows the manifold of right cheek by projecting its reflectance features on the three most dominant principal components. Notice that different classes are overlapped and there are no well defined clusters corresponding to each class. This leads to high correlation both within class and between class spectral reflectance features, making the task of discrimination between the reflectance profiles of different subjects very hard. The manifold of the other five facial regions follows a similar trend.

5.1. Experimental setup

We simulate the settings of a practical real world biometric recognition process and design our experiments to perform recognition on the facial spectral reflectances of the subjects measured in different sessions. For all three databases, we divide the spectral reflectance spectra in gallery and probes sets as follows. For every subject, we randomly select the spectral reflectances measured in one session as probes and the spectra in the rest of the sessions are used as gallery. We repeat the experiments 10 times by randomly generating different gallery probe combinations in each run (10 folds). For KLDA we empirically set the order of the polynomial kernel (parameter β) to 3. The lib-SVM library is used for SVM classifier. We empirically choose the radial basis kernel function with a scale $\gamma = 10^{-2}$ and $C = 100$.

6. Results and discussion

Table 2 summarizes the average recognition rates and standard deviations of 10-fold experiments on our UWA-FSRD. The accuracy of simple Mahalanobis distance based nearest neighbour classifier and simple SVM is low. On the other hand the accuracy increases when the spectral reflectances are projected into discriminative subspaces by performing Sparse Discriminant Analysis or Kernel Linear Discriminant Analysis. The KLDA based classifier performs the best due to its non-linear mapping of the spectral reflectances to a discriminative feature space. Moreover, the accuracies of the spectral reflectances of different facial regions when classified individually is lower than when the regions are combined using the sum rule for

Table 2. Average recognition rates and standard deviations of 10 fold experiments on our UWA-FSRD.

	Forehead	Right Cheek	Left Cheek	Lips	Chin	Hair	Sum Fusion
NN	17.93±3.26	20.73±2.69	24.41±3.28	14.56±1.79	22.70±2.15	10.12±2.50	36.54±3.51
SVM	10.65±3.65	20.31±2.89	16.33±3.41	13.07±1.38	11.22±5.69	10.22±2.64	-
SDA	25.55±3.84	28.09±2.16	24.17±4.79	21.28±2.98	30.22±2.39	15.21±2.86	44.82±5.89
KLDA	23.38±2.82	33.22±2.31	27.68±3.71	22.96±2.69	33.01±2.76	12.97±3.79	**53.83±4.06**

#237187 - $15.00 USD Received 31 Mar 2015; revised 8 May 2015; accepted 15 May 2015; published 1 Jun 2015

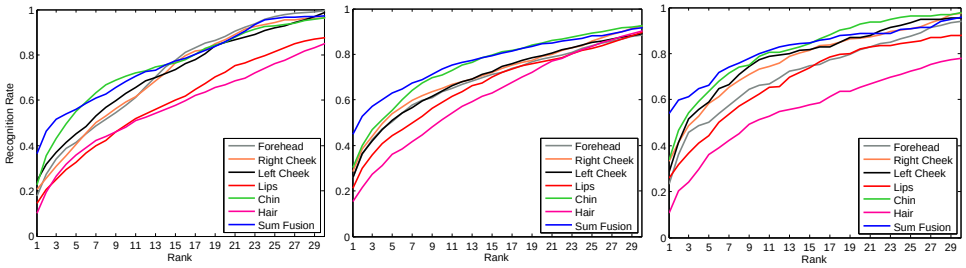

(a) (b) (c)

Fig. 8. Cumulative Match Characteristics Curves of the (a) Mahalanobis (b) SDA and (c) KLDA based classifier on UWA-FSRD database.

score level fusion. The KLDA based classifier achieved a rank-1 recognition rate of 53.83% using the sum based score level fusion of the six facial regions. We also performed recognition experiments by excluding the lips and hair reflectance profiles. The NN, SDA and KLDA classifiers achieved 32.86%, 39.02% and 46.14% accuracies respectively which are lower than that of the combined six regions (Table 2).

Figure 8 gives the Cumulative Match Characteristics (CMC) [34] of different classification methods for 10-fold experiments on our UWA-FSRD. The classification accuracy reaches to its maximum at very higher ranks which suggests the poor performance of spectral reflectances for unconstrained person identification.

Table 3 summarizes the average recognition rates and standard deviations of 10-fold experiments on the facial spectral reflectances in the CMU database. Similar to the results on our spectrometer database, the accuracy of individual facial regions are lower than when combined using the sum rule based score fusion. Compared to our spectrometer based database, the CMU database has lower spectral resolution (step size of 10). Therefore, the classification accuracy of all the algorithms is lower compared to our spectrometer based database. The KLDA based classifier achieves a rank-1 recognition rate of 40.89% on this database.

Figure 9 shows the CMC curves of different classifiers on the facial spectral reflectances in CMU database. The spectral reflectances achieve their highest recognition rates at very high ranks. This further suggests that the strength of spectral reflectance alone is not enough to discriminate faces.

Table 4 summarizes the average recognition rates and standard deviations of 10-fold experi-

Table 3. Average recognition rates (%) and standard deviations of 10 fold experiments on the CMU-HSFD.

	Forehead	Right Cheek	Left Cheek	Lips	Chin	Hair	Sum Fusion
NN	16.94±4.32	15.56±2.36	16.39±1.18	10.33±2.36	12.50±0.39	10.17±1.18	33.89±4.79
SVM	16.06±3.54	19.72±5.11	21.67±1.57	16.11±3.14	15.61±1.18	14.17±1.96	-
SDA	16.11±1.57	11.39±1.18	10.83±5.11	10.08±3.14	13.61±3.54	10.56±2.36	30.28±4.32
KLDA	16.67±4.71	18.61±1.96	16.39±5.11	11.67±1.57	16.96±1.18	13.89±1.96	**40.89±4.71**

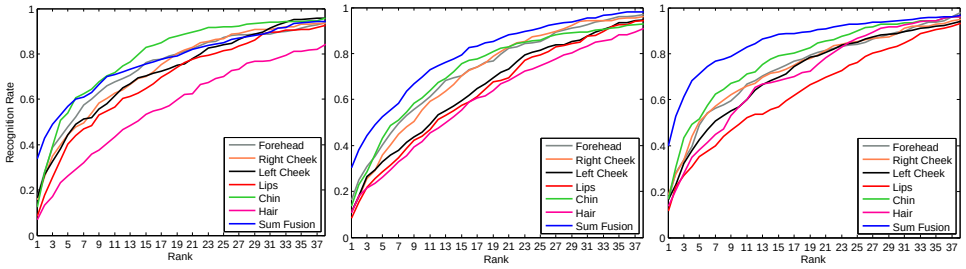

(a) (b) (c)

Fig. 9. Cumulative Match Characteristics Curves of the (a) Mahalanobis (b) SDA and (c) KLDA based classifier on CMU-HSFD database.

#237187 - $15.00 USD Received 31 Mar 2015; revised 8 May 2015; accepted 15 May 2015; published 1 Jun 2015

Table 4. Average recognition rates (%) and standard deviations of 10 fold experiments on the UWA-HSFD.

	Forehead	Right Cheek	Left Cheek	Lips	Chin	Hair	Sum Fusion
NN	11.25±3.54	21.25±4.32	13.75±3.82	11.25±2.05	16.26±2.01	4.00±3.84	20.00±3.58
SVM	13.75±3.66	18.75±4.23	13.75±2.81	7.5±3.84	15.00±2.31	4.50±3.61	-
SDA	13.75±3.25	11.25±3.44	10.00±2.11	6.25±3.58	13.75±3.33	4.78±3.01	**27.50±3.55**
KLDA	10.50±3.85	18.00±2.99	15.50±3.86	11.50±1.75	17.00±2.35	5.00±3.75	25.00±3.92

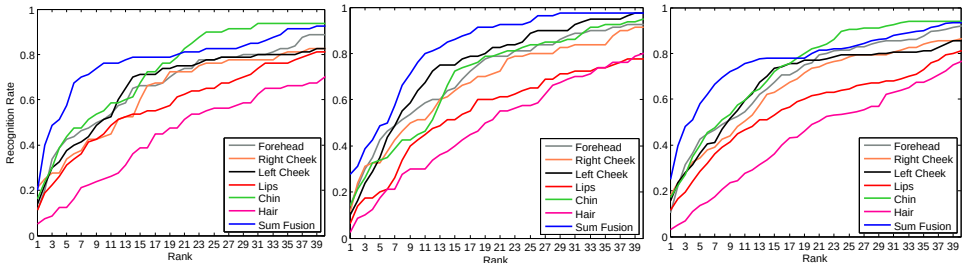

Fig. 10. Cumulative Match Characteristics Curves of the (left) Mahalanobis (center) SDA and (right) KLDA based classifier on UWA-HSFD database.

ments on the facial spectral reflectances in the UWA-HSFD database. The UWA-HSFD covers only the visible range of electromagnetic spectrum and therefore contains lesser information than the CMU database and the proposed spectrometer based database. The spectral resolution is also low compared to our spectrometer database. Therefore, the accuracy of spectral reflectance based face recognition on this database is very low. The SDA based classifier boosts the accuracy by projecting the data to a discriminative subspace. However the rank-1 recognition rate of 27.50% is still not satisfactory.

Figure 10 shows the CMC curves of different classifiers on the facial spectral reflectances in the UWA-HSFD. Similar to the CMU-HSFD and our spectrometer database, the spectral reflectances fail to achieve good rank-1 recognition accuracy.

6.1. Reasons of the low recognition rate

Pan et al. [17] reported 95% rank-1 recognition accuracy using only the facial spectral reflectance and Nearest Neighbour classifier. However, their experiments involved subjects that were imaged in only one session without any time lapse. To further verify this, we repeated our experiments on the UWA spectrometer database (UWA-FSRD) using facial spectral reflectances of the same session in the gallery and probes. We obtained $86.0 \pm 2.9\%$ accuracy in 10-fold experiments using KLDA. Note that this is over three times higher than the different session accuracy given in Table 4.

The main reason of the drop of accuracy from same session to different sessions is that the spectral reflectance of a subject's face can significantly change with location and time depending on the subject's physical conditions such as blood pressure, body water percentage, sweating and the use of cosmetics etc. For example, inflammation caused by infection or irritation can lead to hyperpigmentation i.e. excess production of melanin [35, 36]. Changes in the melanin distribution and oxygen saturation in the hemoglobin can induce significant deviations in the spectral reflectance of the same person [37, 38]. Moreover, ultraviolet exposure of human skin has been shown to increase the epidermal thickness in addition to increasing its melanin content [10, 39, 40]. Similarly, smoking has also been shown to decrease epidermal thickness [41]. Other factors such as the use of cosmetics, along with sensor drift and sensitivity, reduce the discrimination capability of the skin spectral reflectance. Figure 11 shows an example of how the spectral reflectance profiles of the same subject change with time. In this example, the time lapse between the two measurement sessions was three weeks. As the fa-

#237187 - $15.00 USD Received 31 Mar 2015; revised 8 May 2015; accepted 15 May 2015; published 1 Jun 2015

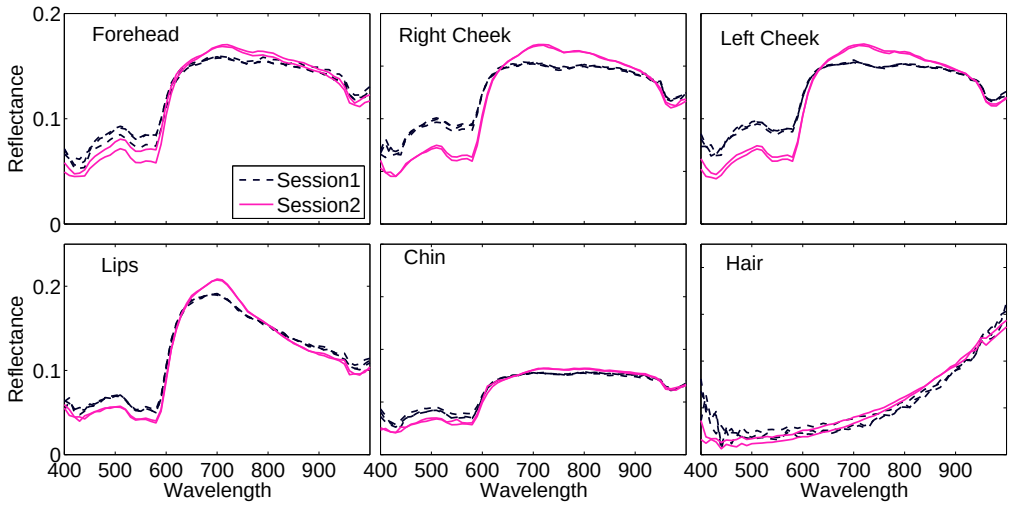

Fig. 11. Variations in the spectral reflectance profiles of the same subject measured in different sessions. In this example, the time lapse between the two sessions was three weeks.

cial spectral reflectance of all the subjects follows a very similar pattern, a small change in the spectra of one subject leads to a large intra-class difference and inter-class correlations. Since the uniqueness of spectral reflectance is poor, the rank-1 recognition rate of spectral reflectance based face recognition is low.

6.2. Significance of results

Although, the number of subjects involved in our study was small, our results are significant because the accuracy of face recognition systems generally decrease when the number of subjects increase. The most significant part of our experiments is that we collected the data using a standard white light source and a high precision spectrometer with 1441 bands covering the visible and infra-red range. Therefore, the only variations that occurred between sessions were due to physical conditions of the skin. Finally, we are making our UWA-FSRD database public so that other researchers can reproduce our results and/or advance this research field.

7. Conclusion

We studied the practical significance of facial spectral reflectance for human identification and introduced a new database acquired with a high precision spectrometer for this purpose. We performed extensive face recognition experiments on the acquired data as well as two public hyperspectral datasets using state-of-the-art face recognition algorithms. Due to the high spectral resolution, the rank-1 recognition rates on our dataset was higher compared to the other two databases. However, the overall recognition rates of the facial spectral reflectance alone for unconstrained face recognition were unsatisfactory. Our experiments show that the spectral reflectance profiles of the human faces follow a similar pattern (see Fig. 5 and Fig. 6). On the average, the between person variations are not significantly different from the within person temporal variations (see Fig. 11). Therefore, we conclude that the spectral reflectance profile alone is not a reliable biometric for person identification. Our future study involves investigating the facial spectral reflectance for gender classification and liveness detection in biometric applications.

Acknowledgment

This research was supported by the Australian Research Council (ARC) grant DP110102399.

#237187 - $15.00 USD Received 31 Mar 2015; revised 8 May 2015; accepted 15 May 2015; published 1 Jun 2015